BMC Complementary Medicine and Therapies

RESEARCH

Open Access

Revealing the multi-target compounds of *Sarcandra glabra* identification and inhibition of novel target genes for the treatment of pancreatic cancer

Xing Liu[1] and Jianghong Ou[2*]

Abstract

Background *S. glabra* has been widely used to treat tumors in traditional Chinese medicine (TCM). However, the specific mechanism of action of *S. glabra* in pancreatic cancer remains unclear. In this study, network pharmacological analysis was used to identify the active components of *S. glabra* and their corresponding targets for the treatment of pancreatic cancer. Furthermore, molecular docking, molecular dynamic simulations, and in vitro experiments were performed to validate the findings.

Methods The active components of *S. glabra* and their corresponding targets for the treatment of pancreatic cancer were identified using the TCMSP database and a literature search. Differentially expressed genes were identified using data from the Gene Expression Omnibus (GEO) database, and their protein–protein interaction (PPI) network was constructed using the STRING platform. The target genes of *S. glabra* were further assessed using Gene Ontology (GO) and Kyoto Encyclopedia of Genes and Genomes (KEGG) analyses in the R software. Subsequently, a protein-protein interaction (PPI) network and a composite target–pathway network were established. The target genes were subjected to survival and mutation analyses. Molecular docking and molecular dynamic simulations were used to validate the interaction between the hub target genes and *S. glabra* in vitro. In addition, cell viability and qRT-PCR verification of *S. glabra* against pancreatic cancer in vitro.

Results A total of 20 active components and 70 targets were identified. Based on the PPI network, *CASP3*, *MMP9*, *CCND1*, *EGF*, *MMP2*, *CASP8*, *ERBB2*, *STAT1*, and *PPARG* were identified as hub target genes. Enrichment analysis showed that *S. glabra* may primarily affect pathways such as p53 signaling, transcriptional dysregulation in cancer, proteoglycans in cancer, pancreatic cancer, and cell cycle. Molecular docking and molecular dynamic simulations indicated stable binding between anhydroicaritin-GSK3B and quercetin-PPARG. In vitro experiments demonstrated that treatment with *S. glabra* significantly inhibited the growth of PANC-1 cells and downregulated expression of *GSK3B* and *PPARG* ($P < 0.05$).

*Correspondence:
Jianghong Ou
617325059@163.com

Full list of author information is available at the end of the article

Conclusion This study demonstrates the potential of *S. glabra*, a herb in traditional Chinese medicine, for treating pancreatic cancer. The findings provide insights into the mechanism of action of the active ingredients of *S. glabra*, offering a strong theoretical foundation for its various clinical applications.

Clinical trial number Not applicable.

Keywords *Sarcandra glabra*, Pancreatic cancer, Network pharmacology, Molecular docking, Molecular dynamic simulations

Introduction

Pancreatic cancer (PC) is the third leading cause of cancer-related deaths in both men and women, with a 5-year survival rate of only 13%, which is the lowest of all tumors [1]. According to a statistical report from China, PC was the eighth most common cancer and the sixth leading cause of cancer-related deaths in 2022, suggesting a close alignment between the incidence and mortality rates. The incidence and mortality rates of PC are higher in men than in women, indicating sex disparity [2]. By 2030, PC is projected to become the second leading cause of cancer-related deaths in the United States of America, with the disease burden being highest in high-income countries [3, 4]. The poor prognosis of PC is primarily attributed to the lack of specific early-stage symptoms and effective screening methods, owing to which most patients are diagnosed at advanced stages. Despite successful surgery, more than 80% of patients eventually experience local recurrence or metastasis [5]. Although advancements have been made in conventional chemotherapy, radiotherapy, and palliative treatment for PC, early diagnosis and prompt intervention are necessary for reducing the mortality rate. Given that molecular mechanisms driving the progression of PC remain elusive, identifying potential molecular signatures is essential for understanding these mechanisms and developing promising drugs.

In addition to surgery and radiotherapy, chemotherapy is commonly used to treat malignant tumors. However, chemotherapeutic drugs have side effects, and patients may develop drug resistance over time. Therefore, identifying less toxic and more effective antitumor drugs is crucial. Traditional Chinese medicine (TCM) is effective in preventing and treating malignant tumors, alleviating clinical symptoms, reducing the side effects of radiotherapy, reversing drug resistance, and improving the quality of life. *Sarcandra glabra*, a Chinese herb, has been shown to control cancer development, improve the quality of a patient's life, and alleviate clinical symptoms. Modern pharmacological studies have shown that *S. glabra* has various biological properties, including antioxidant, antibacterial, antiviral, antimalarial, antithrombocytopenic, antitumor, anti-inflammatory, immunomodulatory, hepatoprotective, hypoglycemic, and hypolipidemic properties [6, 7]. However, studies investigating the therapeutic potential of *S. glabra* in PC are limited. Therefore, the pharmacological role of the active components of *S. glabra* in PC should be comprehensively analyzed using scientific and technological approaches.

In 2007, Hopkins introduced the concept of "network pharmacology," which integrates principles from systems biology, genomics, proteomics, and other disciplines. This approach involves the use of high-throughput genomic data analysis, computer simulations, and network databases to reveal the close interactions among drugs, genes, targets, and diseases [8]. Understanding these interactions may help determine the mechanisms of action of drugs, assess their efficacy, and predict their adverse effects to identify effective and less toxic drugs [9]. Given the complexity of tumors, the combination of network pharmacology and traditional Chinese medicine (TCM) may represent a more systematic and effective approach to preventing and treating tumors [10, 11]. The holistic and systematic nature of network pharmacology aligns well with the multi-component, multi-target, and multi-pathway characteristics of TCM. Consequently, using network pharmacology to investigate the mechanisms of action of traditional Chinese medications has emerged as a prevalent research strategy in recent years. For instance, in a study, network pharmacological analysis and experimental validation revealed TNF, MMP9, STAT3, PIK3CA, and ERBB2 as key targets of icariin for the treatment of ovarian cancer. In addition, GO and KEGG enrichment analyses revealed that icariin inhibited the proliferative, migratory, and invasive abilities of ovarian cancer cells primarily by suppressing the PI3K/AKT signaling pathway [12]. Similarly, a study on *Rheum palmatum* L. and its active compounds demonstrated that the compounds inhibited the proliferative and colony-forming abilities of lung cancer A549 cells by inducing apoptosis, providing insights into the therapeutic effects of *Rheum palmatum* L. against lung cancer from a systems biology perspective [13].

In this study, network pharmacological analysis was used to identify the active components and potential targets of *S. glabra* in the treatment of PC. Multi-component, multi-target models were constructed to elucidate the complex interactions between the active components and target proteins. Microarray data analysis, survival analysis, molecular docking, and cellular experiments

were performed to validate the findings. Subsequently, 100-ns all-atom molecular dynamic (MD) simulations and MMBBA/GBSA analysis were performed to investigate the conformation, stability, and mechanism of the binding between active components and target proteins. Furthermore, in vitro experiments validated the therapeutic potential of the active components of *S. glabra* in PC. To the best of our knowledge, this study is the first to investigate the efficacy and mechanism of action of *S. glabra* in the treatment of PC. The findings provide a theoretical basis for further research and may facilitate the identification of novel drugs for PC. The flow chart of the study is shown in Fig. 1.

Materials and methods

Virtual screening of active components

The bioactive components of *S. glabra* were identified using data from TCMSP (https://old.tcmsp-e.com/tcmsp.php) [14]. Targets were predicted and selected based on oral bioavailability (OB) of ≥30% and drug-likeness (DL) of ≥0.18 [15, 16, 17]. The primary pharmacological components of *S. glabra* were included in subsequent analysis.

Screening of potential target genes

Three microarray datasets (GSE15471, GSE28735, and GSE62452) were obtained from the Gene Expression Omnibus (GEO) database (https://www.ncbi.nlm.nih.gov/geo/) by NCBI using the search term "pancreatic cancer". These datasets were selected owing to their inclusion of tissue samples from both healthy individuals and patients with PC. The GSE15471 dataset, submitted by Badea et al. [18], contained 78 samples (36 healthy individuals and 42 patients with PC). The GSE28735 dataset, submitted by Hussain [19], contained 90 samples (45 healthy individuals and 45 patients with PC), whereas the GSE62452 dataset, also submitted by Hussain [20], contained 130 samples (61 healthy individuals and 69 patients with PC). The limma package (https://www.bioconductor.org/packages/release/bioc/html/limma.html) in R was used to process data and identify differentially expressed genes (DEGs) with adjusted *P*-values of <0.05 and|log2(fold change)| values of ≥1. The identified DEGs

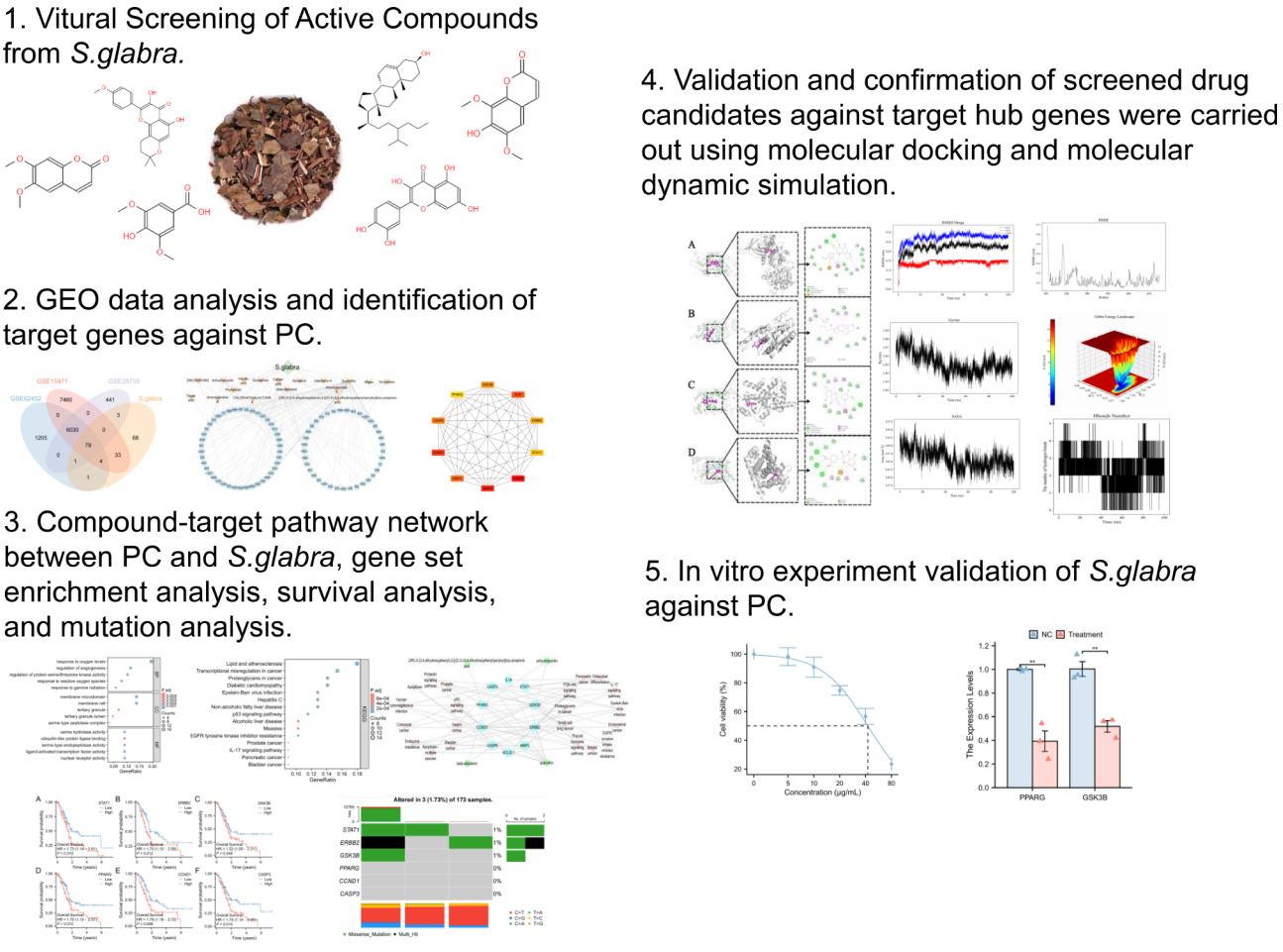

Fig. 1 Flowchart of the network pharmacology study of *S. glabra* for the treatment of PC

Table 1 The ID, DL and OB of compounds in *S. glabra*

Mol ID	Molecule Name	MW	DL	OB(%)
MOL000358	Beta-sitosterol	414.79	0.75	36.91
MOL000359	Sitosterol	414.79	0.75	36.91
MOL004373	Anhydroicaritin	368.41	0.44	45.41
MOL004568	Engelitin	434.43	0.70	36.27
MOL007132	(2R)-3-(3,4-dihydroxyphenyl)-2-[(Z)-3-(3,4-dihydroxyphenyl) acryloyl]oxy-propionic acid	360.34	0.35	109.38
MOL007742	Istanbulin-A	264.35	0.20	80.10
MOL007743	ZINC00391893	270.30	0.20	41.92
MOL007744	CHLORANTHALACTONE A	228.31	0.18	41.72
MOL007747	Chloranoside a_qt	262.33	0.23	84.11
MOL000098	Quercetin	302.25	0.28	46.43
MOL000044	Atractylenolide II	232.35	0.15	47.50
MOL000178	Atractylenolide III	248.35	0.17	31.66
MOL005723	Phytodolor	222.21	0.10	52.32
MOL001999	Scoparone	206.21	0.09	74.75
MOL005021	Mipax	194.20	0.06	57.40
MOL000223	Caffeic acid	180.17	0.05	25.76
MOL001807	Cedar acid	198.19	0.06	47.78
MOL000114	Vanillic acid	168.16	0.04	35.47
MOL000040	Scopoletol	192.18	0.08	27.77
MOL000602	Fumaric acid	116.08	0.01	17.74

were considered potential PC-associated targets. A Venn diagram was generated to identify overlapping targets of interest [21]. To standardize UniProt IDs to official gene symbols, the species "*Homo sapiens*" was specifically selected in the UniProt database (https://www.uniprot.org/) [22].

Network construction

The Search Tool for Retrieval of Interacting Genes (STRING) (https://cn.string-db.org/, version 12.0) platform was used to establish a PPI network [23] of the targets of *S. glabra* against PC. Only experimentally validated interactions with a composite score of ≥ 0.4 were considered significant. The PPI network was visualized using the Cytoscape software (https://cytoscape.org/, version 3.7.2) [24]. The top 10 hub target genes of *S. glabra* were identified, and the Cytohubba plug-in was used to identify anti-PCs for constructing a regulatory network [25].

Functional annotation and pathway analysis

To investigate the biological processes and pathways involved in the therapeutic mechanisms of *S. glabra* in PC, GO functional annotation and KEGG pathway enrichment analyses were performed using the publicly available DAVID database (https://david.ncifcrf.Gov/tools.jsp) [26]. The search focused on common target gene symbols in "*Homo sapiens*". Enrichment analysis encompassed biological processes (BPs), cellular components (CCs), molecular functions (MFs), and KEGG pathways, with a corrected *P*-value of < 0.05 indicating significant enrichment. Results were visualized using the ggplot2 package in R.

Validation of the expression of hub genes in XENA database

The expression of hub genes was validated using RNA-seq data from TCGA and GTEx. The dataset included 167 normal tissue samples from GTEx, 4 paraneoplastic tissue samples from TCGA, and 179 tumor tissue samples from TCGA. All data were obtained from the XENA database and processed uniformly using the Toil tool (https://gdc.xenahubs.net). Statistical analysis was performed using the Wilcoxon rank-sum test, with a *P*-value of < 0.05 indicating statistical significance.

Survival, mutation and immune infiltration analysis

The survival package was used to construct a proportional hazards regression model for each hub gene. Fitted survival regression was performed, and the results were visualized using the survminer and ggplot2 packages [27]. The prognostic value of specific genes was evaluated through survival analysis based on their expression levels. Kaplan–Meier (KM) curves were plotted using the R package (https://www.bioconductor.org/packages/release/bioc/html/kmcut.html) to assess the correlation between the hub genes and the overall survival of patients with PC. Hub genes with *P*-values of < 0.05 were considered statistically significant. The mutation data containing somatic variants were detected by using the "maftools" R package (https://www.bioconductor.org/packages/release/bioc/html/maftools.html) [28], followed by the calculation of TMB. The ssGSEA algorithm in R software (https://www.bioconductor.org/packages/release/bioc/html/GSEABase.html) was utilized to evaluate 24 immune cell types within the TME of each sample [29]. The R package "RCircos" (https://cran.r-project.org/web/packages/RCircos/RCircos.pdf) was used to evaluate the correlation and chromosomal localization of specific genes.

Analysis of the prognostic and diagnostic value of hub genes

To assess the accuracy of the independent survival prognosis model, a time-dependent ROC curve was plotted using the sample data from the "timeROC" R package (https://www.bioconductor.org/). The survival prediction performance of these six genes in PAAD patients at 1, 3, and 5 years was evaluated, respectively. Diagnostic accuracy was defined as follows: low, AUC values of 0.5–0.7; moderate, AUC values of 0.7–0.9; high, AUC values of > 0.9.

Table 2 Potential targets of *S. glabra* and pancreatic cancer

NO.	Target	NO.	Target	NO.	Target	NO.	Target	NO.	Target
1	PTGS1	15	NR3C2	29	MMP2	43	IL1A	57	ERBB3
2	HSP90AA1	16	PPARG	30	TNFSF15	44	MPO	58	NPEPPS
3	KCNH2	17	ESR2	31	AHSA1	45	PSMD3	59	RASA1
4	ADRA1A	18	GSK3B	32	POR	46	SLC2A4	60	CA4
5	SLC6A4	19	CDK2	33	TOP1	47	DCAF5	61	PKIA
6	OPRM1	20	CHEK1	34	STAT1	48	NR1I3	62	DCT
7	GABRA1	21	F7	35	RUNX1T1	49	CHEK2	63	CA1
8	BAX	22	KDR	36	CDK1	50	INSRR	64	SLC6A2
9	CASP3	23	CCNA2	37	ERBB2	51	CLDN4	65	MAOA
10	CASP8	24	GRIA2	38	ACACA	52	PPARA	66	ADRB1
11	PRKCA	25	AKR1B1	39	CYP1A1	53	PPARD	67	ADRA2C
12	NCOA2	26	CCND1	40	ICAM1	54	RUNX2	68	ADRA1D
13	PON1	27	BCL2L1	41	NR1I2	55	CTSD	69	SELP
14	MAP2	28	EIF6	42	IFNGR1	56	IRF1	70	RAC1

Molecular docking

The hub targets identified from the PPI network and genes with diagnostic value were selected as receptors and ligands for molecular docking, respectively. The crystal structures of receptor proteins were obtained from the RCSB PDB database [30], and water molecules were removed using the PyMOL (version 2.4.1) software. The optimized receptor proteins were imported into the AutoDock Tools (version 1.5.6) software for hydrogenation and charge calculations, and the output file was saved in the pdbqt format. The 2D structures of ligands were obtained from the PubChem database and converted to 3D structures using the ChemBio3D Ultra (version 17.0) software. The 3D structures of the ligands were saved in the mol2 format, imported into AutoDock Tools, and saved in the pdbqt format. Molecular docking was performed using the AutoDock Vina (version 1.1.2) software [31], and the results were analyzed and visualized using PyMOL [32].

Molecular dynamic simulations

The Gromacs (version 2022.3) software was used for molecular dynamic simulations [33, 34]. For the preprocessing of small molecules, AmberTools22 was used to apply GAFF, whereas Gaussian 16 W was used for hydrogenation and the calculation of RESP. The resulting data were integrated into the topology file of the molecular dynamic system. Simulations were performed at a constant temperature of 300 K and atmospheric pressure of 1 Bar. The Amber99sb-ildn force field was used, with water molecules serving as the solvent (Tip3p water). The simulation system was subjected to energy minimization using the steepest descent method, followed by equilibration in the isothermal isovolumic ensemble (NVT) and isothermal isobaric ensemble (NPT) for 100,000 steps each, with a coupling constant of 0.1 ps and a duration of 100 ps. Subsequently, a free molecular dynamic simulation of 100 ns was performed, consisting of 5,000,000 steps with a step length of 2 fs. After simulation, the software's built-in tool was used to analyze the trajectory and calculate parameters such as root-mean-square deviation (RMSD), root-mean-square fluctuation (RMSF), protein rotation radius for each amino acid trajectory, free energy (MMGBSA), and free energy topography.

Preparation of *S. glabra* extracts

The whole *S. glabra* herb was purchased and subjected to three rounds of reflux extraction with 85% ethanol. The combined extracts were concentrated using a rotary evaporator to obtain a solvent-free extract. Subsequently, the extract was vacuum-dried to obtain a powder, which was referred to as *S. glabra* extract. For subsequent experiments, 0.5 g of *S. glabra* extract was weighed and mixed with 1 mL of autoclaved distilled water to achieve a concentration of 0.5 g/mL. The resulting solution was filtered, sterilized, and stored in a refrigerator at 4℃ until further use.

Cell culture

The PC cell line PANC-1 was procured from BeiNaChuangLian Biotechnology Co., Ltd. (Henan, China). The cells were cultured in Dulbecco's modified Eagle medium supplemented with 10% fetal bovine serum and maintained in a humidified incubator with 5% CO_2 at 37 °C. Only exponentially growing cells were used for subsequent experiments. The cell culture media and supplements were purchased from HyClone.

Cell counting kit-8 assay

PANC-1 cells were seeded in 96-well plates at a density of 1×10^4 cells/well. The cells were treated with varying concentrations of *S. glabra* extracts (0, 5, 10, 20, 40, and 80 μg/mL) for 48 h. Subsequently, 10 μL of the cell counting kit-8 (CCK-8) reagent (Dojindo, Kyushu, Japan) was

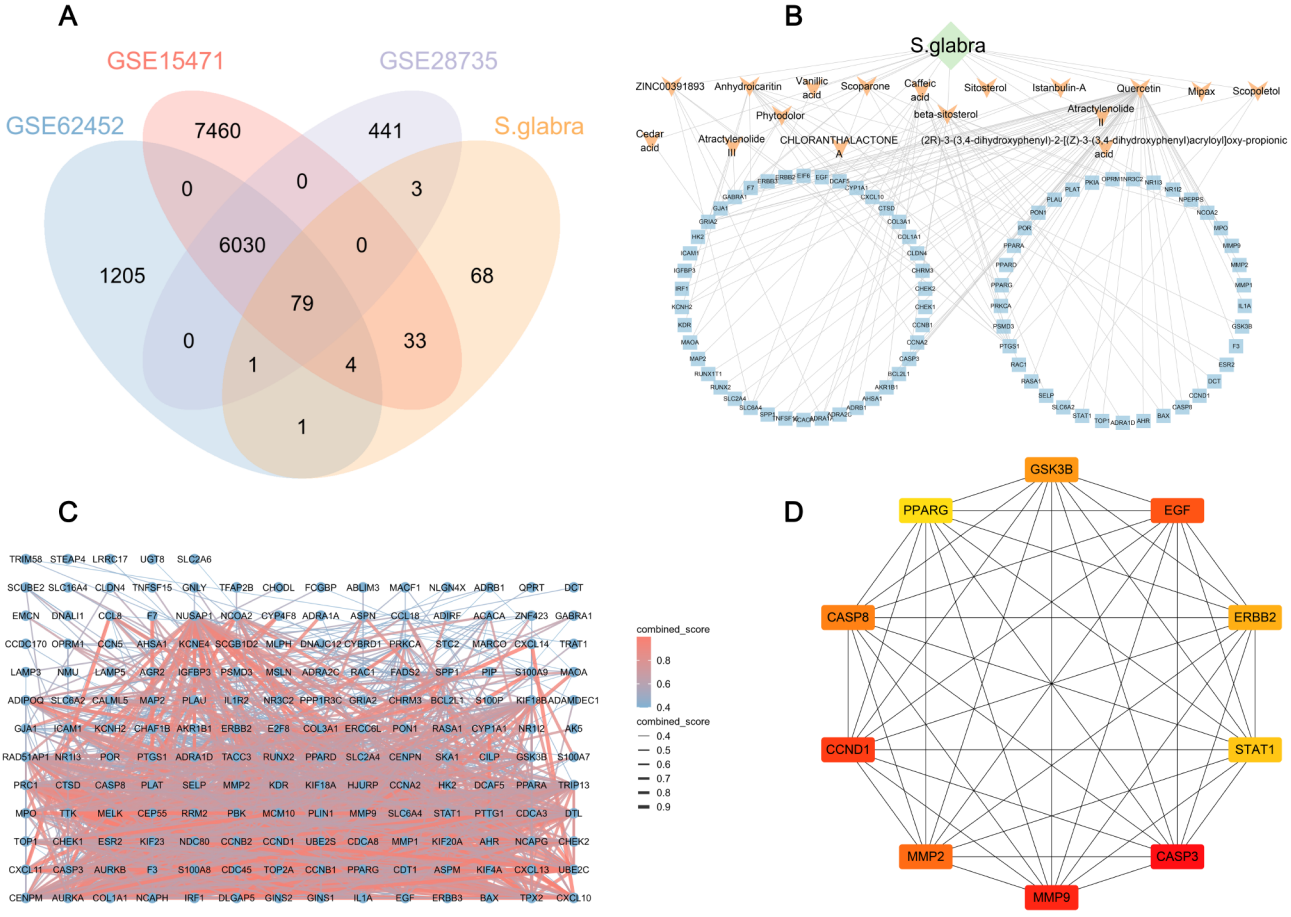

Fig. 2 Collecting active compounds of *S. glabra* and prediction of key therapeutic targets for PC. **A**: Venn diagram of the target gene of *S. glabra* and PC. **B**: *S. glabra* component target network diagram. **C**: The interaction network between targets. **D**: The 10 hub genes were determined using CytoHubba

added to each well. The plates were incubated at 37 °C for 3 h, and absorbance was measured at a wavelength of 450 nm.

Real-time reverse transcription polymerase chain reaction

PANC-1 cells were treated with *S. glabra* extracts at concentrations of 30 μg/mL for 24 h. Total RNA was extracted from the cells using chloroform and Trizol (Invitrogen, USA). The extracted RNA was used to synthesize cDNA according to the manufacturer's instructions. The cDNA was used for real-time polymerase chain reaction (qPCR) using a SYBR premix kit (Vazyme Biotech Co.,Ltd, China). Each real-time reverse transcription polymerase chain reaction (qRT-PCR) experiment was repeated at least three times. The primer sequences used for PCR are mentioned in Supplement Table 1, Additional File 1.

Results

Identification of active ingredients and prediction of their targets

After screening, filtering, and removal of duplicates, a total of 20 active components of *S. glabra* were identified, including beta-sitosterol, sitosterol and cedar acid (Table 1). OB values of ≥ 30% indicated that the components could be absorbed and utilized by the body after consumption. Although the OB values of scopoletol and fumaric acid were < 30%, literature search showed that these components had significant anticancer activity. A total of 394 potential target genes of the 20 active components were identified using the TCMSP database. Subsequently, PC-associated target genes were obtained from the GEO database. In the GSE15471 dataset, 1,401 of 21,655 genes, including 1,212 upregulated and 189 downregulated genes, met the screening criteria. In the GSE28735 dataset, 443 of 28,869 genes, including 172 upregulated and 271 downregulated genes, met the screening criteria. In the GSE62452 dataset, 323 of 33,297 genes, including 120 upregulated and 203 downregulated genes, met the screening criteria. Subsequently, a Venn

diagram was constructed to intersect the target genes of the active components with PC-associated target genes to identify overlapping genes. Eventually, a total of 70 targets of *S. glabra* against PC were identified (Table 2), and these targets and corresponding active components were selected for subsequent analysis (Fig. 2A, B).

Network analysis

Cytoscape was used to construct and visualize a PPI network to elucidate the multi-target mechanism of action of *S. glabra* in the treatment of PC (Fig. 2C). The network comprised 97 nodes and 223 edges, with nodes representing target genes and their corresponding active components and edges representing interactions between the nodes. Analysis of the network revealed that quercetin exhibited the highest number of interactions within the network (59), followed by β-sitosterol (15), caffeic acid (13), anhydroicaritin (12), scoparone (7), ZINC00391893 (6), phytodolor (4), scopoletol (4), vanillic acid (3), istanbulin A (1), and cedar acid (1). Each active component was found to have multiple targets, suggesting that the components exert synergistic effects against PC. Subsequently, a PPI network of 79 overlapping genes was constructed using the STRING database. The network demonstrated close interactions between various target genes, represented as nodes, during disease progression (Supplement Table 2, Additional File 2). Notably, no target genes were directly related to other genes within the network, supporting the strong relationship among target genes. CytoHubba analysis revealed *CASP3* (47), *CASP8* (28), *CCND1* (37), *EGF* (38), *ERBB2* (34), *GSK3B* (37), *MMP2* (34), *MMP9* (40), *PPARG* (36), and *STAT1* (25) as hub target genes (Fig. 2D).

GO and KEGG enrichment analyses

GO functional annotation and KEGG pathway enrichment analyses were performed to investigate the mechanism of action of *S. glabra* in the treatment of PC. A total of 717 BPs, 25 CCs, 58 MFs, and 77 KEGG pathways were identified based on adjusted *P*-values < 0.05. The results were visualized on bubble plots (Fig. 3A, Supplement Table 3, Additional File 3). According to GO analysis, the target genes of *S. glabra* were associated with BPs such as responses to oxygen levels, kinase activity, regulation

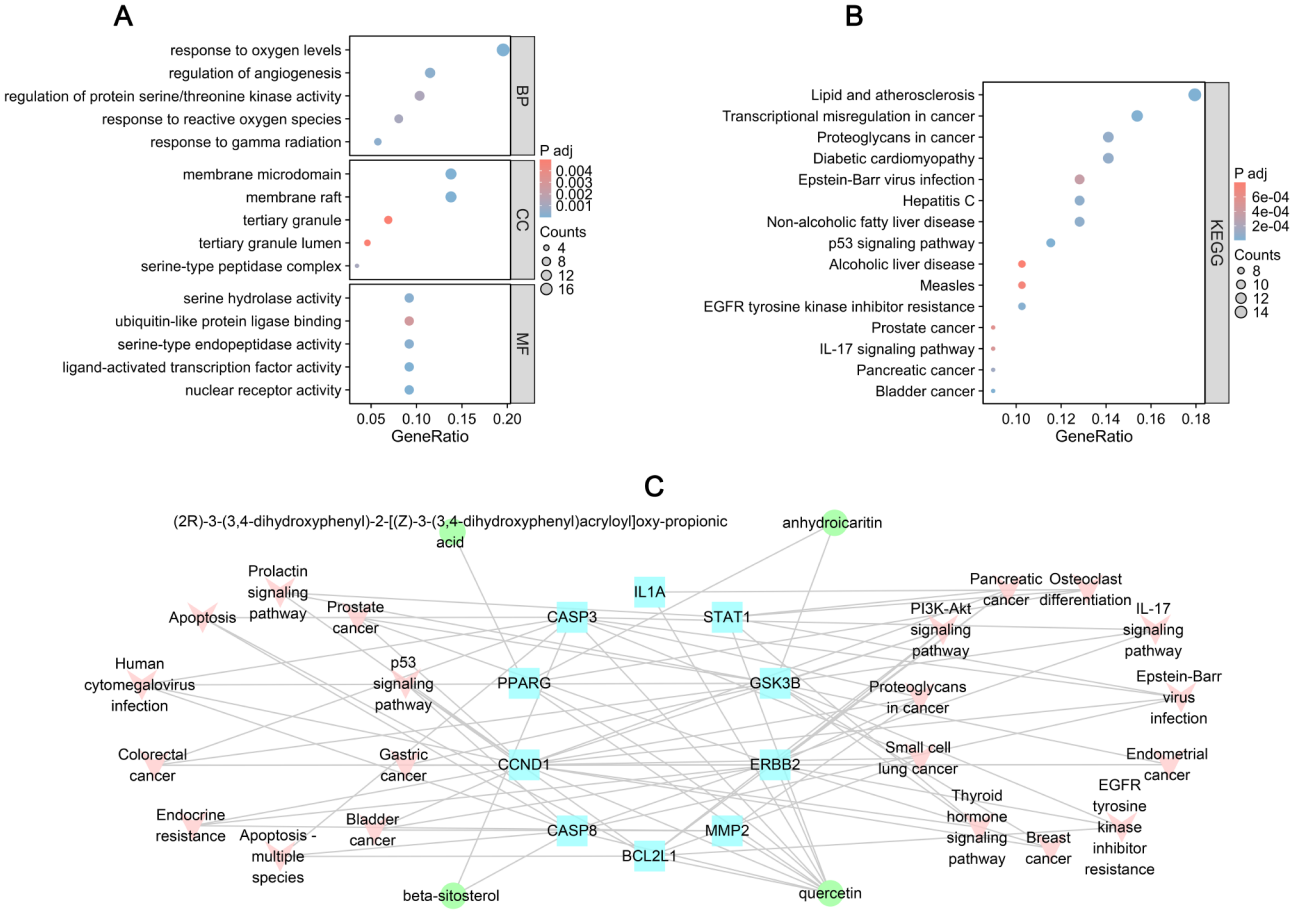

Fig. 3 Results of *S. glabra* targets enrichment analysis. **A**: GO enrichment analysis. **B**: KEGG enrichment analysis. **C**: Component-target-pathway interaction network construction

of angiogenesis, reactive oxygen species response, and response of gamma radiation. Additionally, the target genes were involved in MFs such as nuclear factor binding, ubiquitin-like protein ligase binding, transcription factor activity, and serine hydrolase activity (Fig. 3B, Supplement Table 4, Additional File 4). Furthermore, KEGG analysis showed that the target genes were associated with transcriptional misregulation in cancer, proteoglycans in cancer, Diabetic cardiomyopathy, pancreatic cancer, cell cycle, IL-17 signaling pathway, p53 signaling pathway, Epstein–Barr virus infection, cellular senescence, measles, hepatitis C, EGFR tyrosine kinase inhibitor resistance, influenza A, lipid and atherosclerosis, bladder cancer and alcoholic liver disease (Fig. 3C).

Survival, mutation and immune infiltration analysis

KM curves were plotted to evaluate the relationship between the hub target genes and patient survival in PC. The results showed a significant difference in survival rates between patients with high and low expression of *STAT1*, *ERBB2*, *GSK3B*, *PPARG*, *CCND1*, and *CASP3* ($P < 0.05$), suggesting the potential involvement of these genes in the survival of patients with PC (Fig. 4). The AUC values were calculated to validate the prognostic value of these genes in PC (Fig. 5). Furthermore, the expression levels of these genes exhibited substantial differences between the normal and PC cohorts of TCGA (Fig. 6A). Correlation analysis of these genes revealed positive correlations (Fig. 6B). The genetic map displayed the chromosomal locations of the copy number variation (CNV) genes associated with six genes (Fig. 6C). Notably, ERBB2 exhibited high amplification, while CASP3 exhibited a higher frequency of deletions (Fig. 6D). In addition, we evaluated the SNP alteration among the hub genes and observed that the mutation frequencies were 1.73%. *STAT1*, *ERBB2* and *GSK3B* have a higher SNP alteration than *PPARG*, *CCND1* and *CASP3* (Fig. 6E). The correlation between 24 types of immune cells and survival-related genes is illustrated in Fig. 6F, highlighting their significant association, particularly with *STAT1*.

Molecular Docking of hub genes with active components

Based on microarray data and survival analysis, molecular docking was performed between the survival-related genes *STAT1*, *ERBB2*, *GSK3B*, *PPARG*, *CCND1*, and *CASP3* and the small-molecule active components quercetin, anhydroicaritin, and beta-sitosterol. The non-covalent interactions between proteins and their corresponding drug molecules were analyzed online using PLIP [35]. The results can be found in Supplement Table 5, Additional File 5.

The above mentioned three active components exhibited hydrogen bonding, Pi-Pi stacking, and van der Waals interactions with receptor proteins. As shown in Fig. 7A,

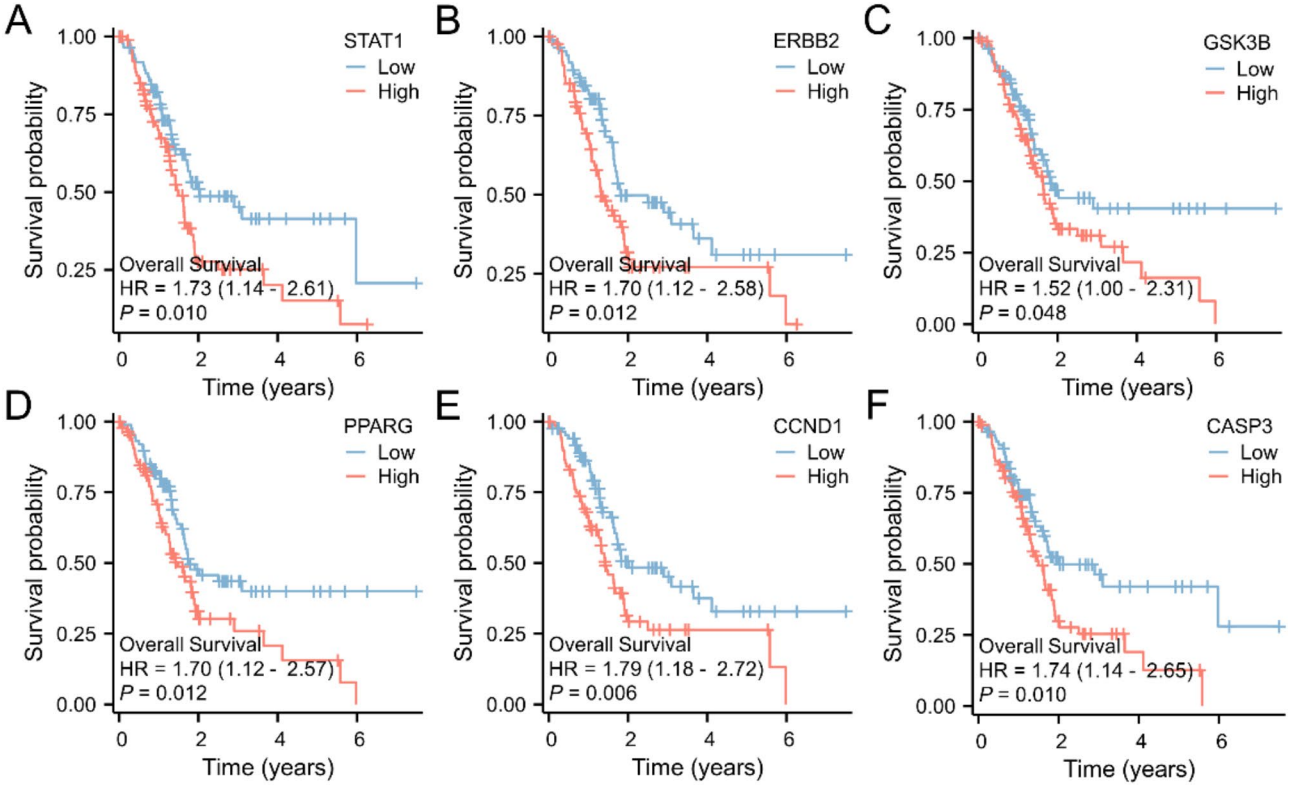

Fig. 4 K-M survival analysis of drug targets in the low or high expression level. **A**: *STAT1*. **B**: *ERBB2*. **C**: *GSK3B*. **D**: *PPARG*. **E**: *CCND1*. **F**: *CASP3*

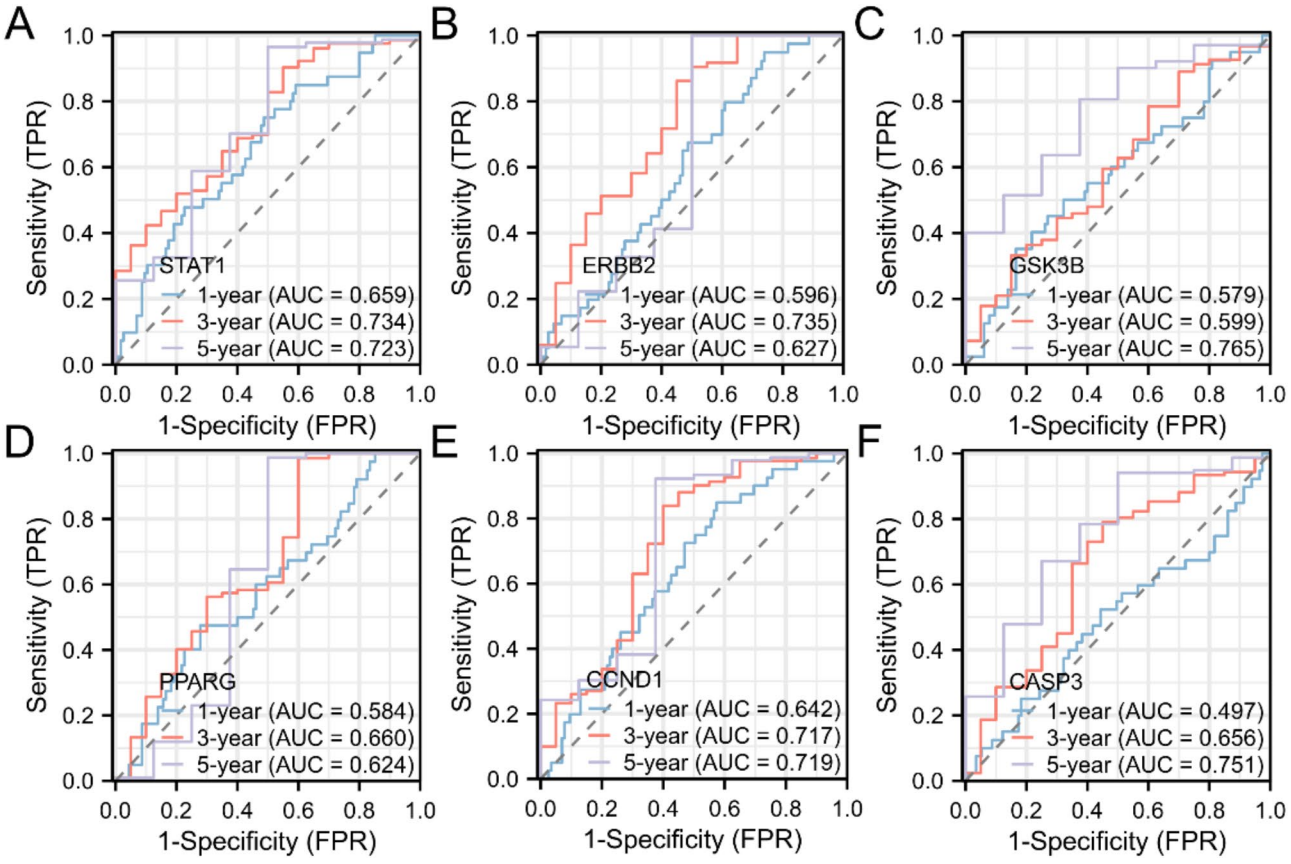

Fig. 5 ROC curves for 1-, 3-, 5-year OS by the component target genes. **A**: *STAT1*. **B**: *ERBB2*. **C**: *GSK3B*. **D**: *PPARG*. **E**: *CCND1*. **F**: *CASP3*

anhydroicaritin could stably bind to the GSK3B protein with a binding affinity of -8.653 kJ/mol, forming hydrogen bonds with the side chains of ASN A:95 and ARG A:96 and engaging in Pi-Pi stacking with PHE A:67. Similarly, beta-sitosterol could stably bind to the CASP3 protein with a binding affinity of -7.737 kJ/mol, forming hydrogen bonds with the side chains of PHE A:256, TRP A:206, TRY A:204, CYS A:163, and HIS A:121 to facilitate Pi-Pi stacking (Fig. 7B). Quercetin could stably bind to the PPARG protein with a binding affinity of -8.742 kJ/mol, forming hydrogen bonds with the side chains of SER A:342 and GLU A:259, Pi-alkyl interactions with ILE A:341 and ARG A:288, and Pi with PHE A:264 (Fig. 7C). Quercetin could stably bind to the CCND1 protein with a binding affinity of -7.189 kJ/mol, forming hydrogen bonds with the side chains of PHE A:78, CYS A:73, and GLU A:74 and Pi-alkyl interactions with the side chains of CYS A:68 and ALA A:187. Additionally, it formed Pi-alkyl interactions with the side chain of GLU A:69 to form a Pi-anion (Fig. 7D). Quercetin could stably bind to the STAT1 protein with a binding affinity of -7.57 kJ/mol, establishing hydrogen bonds with the side chains of ASP A:365 and VAL A:362 and Pi-alkyl interactions with the side chains of ILE A:382 and LYS A:379. Furthermore, Pi-alkyl interactions with the side chains of HIS A:386 led to the formation of Pi-Pi stacking (Fig. 8A). Quercetin could stably bind to the ERBB2 protein with a binding affinity of -7.758 kJ/mol. It interacted with HIS B:267, ARG A:258, GLN A:281, HIS A:248, THR B:273, and TRY B:274, forming hydrogen bonds with the side chains of PRO B:269, ARG A:258, and ALA B:270. In addition, it exhibited Pi-alkyl and Pi-Pi stacking interactions with the side chain of HIS A:248 and Pi-cation interactions with the side chain of ARG A:258 (Fig. 8B). Quercetin could stably bind to the CASP3 protein with a binding affinity of -6.659 kJ/mol, establishing hydrogen bonds with the side chains of PHE A:275, ASP A:228, LEU A:223, and LYS A:224 and Pi-alkyl interactions with the side chain of ALA A:227 and forming a Pi-anion (Fig. 8C). These findings suggest that the hub genes are promising targets of *S. glabra* for the treatment of PC. Future studies should focus on identifying the binding sites of the active components *of S. glabra* in hub genes.

Molecular dynamic simulations

To investigate protein–ligand stability and structural flexibility of PPARG, GSK3B, and their docking complexes, 100-ns MD simulations were performed using Gromacs. MD simulation reveals positional changes between the conformation of a small molecule during the simulation

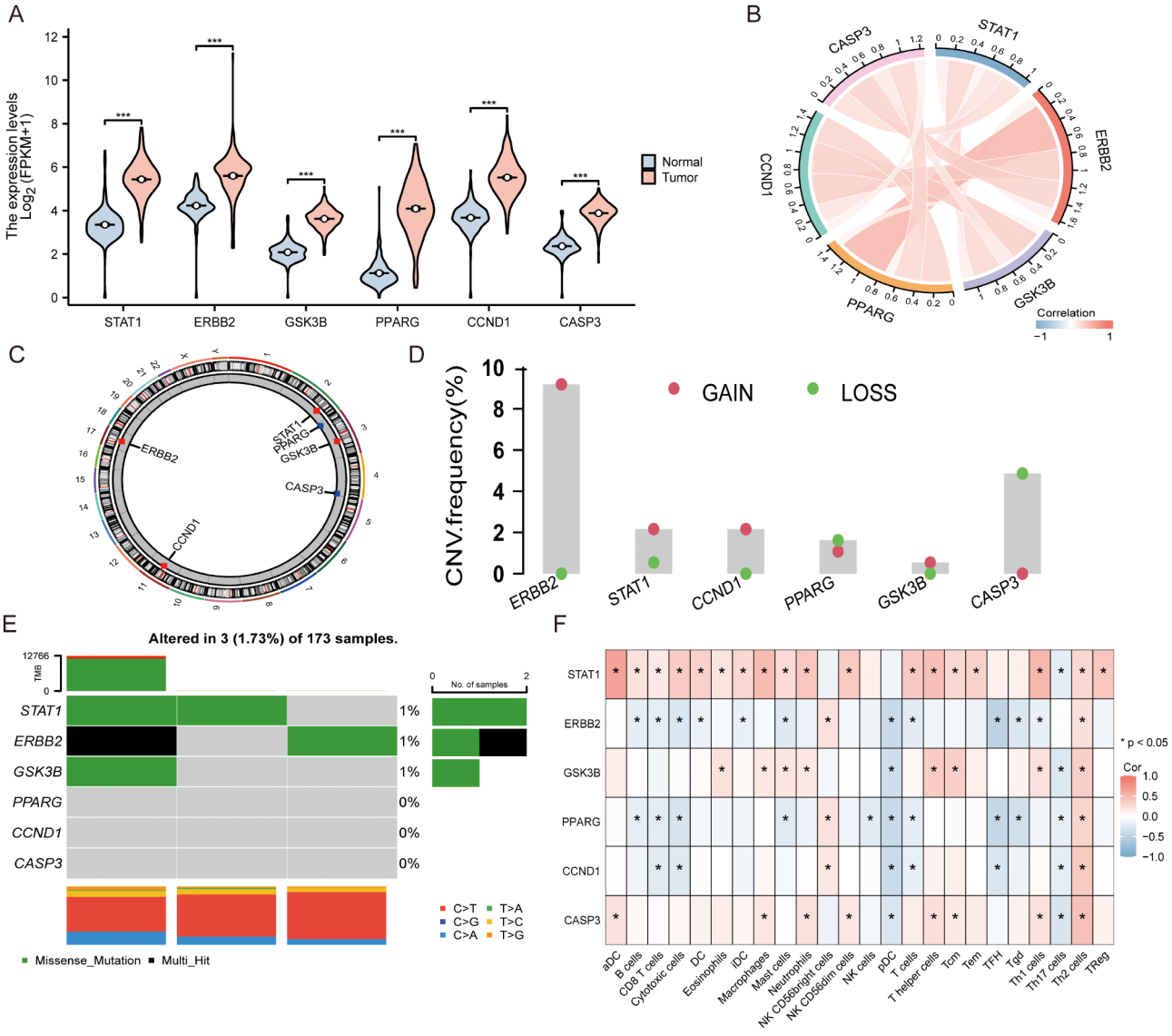

Fig. 6 Expression of *S. glabra* target genes in PC. **A**: Comparison of expression between normal and tumor tissues of TCGA PAAD samples. **B**: Spearman correlations between genes. The blue represents negative regulation; the red represents positive regulation. **C**: Distribution of *S. glabra* target genes on chromosomes. **D**: CNV values for target genes in PC specimens. **E**: Mutation frequencies of the 6 target genes in 173 PC specimens. **F**: Correlation between immune infiltration and target genes. *$P < 0.05$

and its initial conformation. In this study, all analyzed complexes exhibited intrinsic stability (Figs. 9 and 10). In this study, RMSD, a kinetic metric, was used to analyze the stability of protein–ligand binding from a thermodynamic perspective. The RMSD values of all complexes showed a gradual increase with minimal fluctuation over 0–100 ns. GSK3B interacting with anhydroicaritin had a larger RMSD value in the first 50 ns before being stabilized (Fig. 9A). Similarly, PPARG interacting with quercetin had a larger RMSD value in the initial 15 ns, which stabilized thereafter (Fig. 10A). The RMSD values consistently remained within a small amplitude range, indicating relatively stable protein–small molecule binding.

The MM/GBSA method was used to calculate binding free energy and various other energies, particularly van der Waals (VDWAALS) interactions, electrostatic potential energy (EEL), and solvation free energy (ΔGsolv). As shown in Table 3, anhydroicaritin exhibited stronger EEL and VDWAALS interactions. In particular, VDWAALS interactions were dominant, favoring the binding between anhydroicaritin and GSK3B. Furthermore, quercetin exhibited stronger VDWAALS interactions and ΔGgas, which support its binding to PPARG. The calculated free energies of binding for both GSK3B-anhydroicaritin and PPARG-quercetin complexes were low, indicating successful binding between the small molecules and proteins. To identify key residues interacting

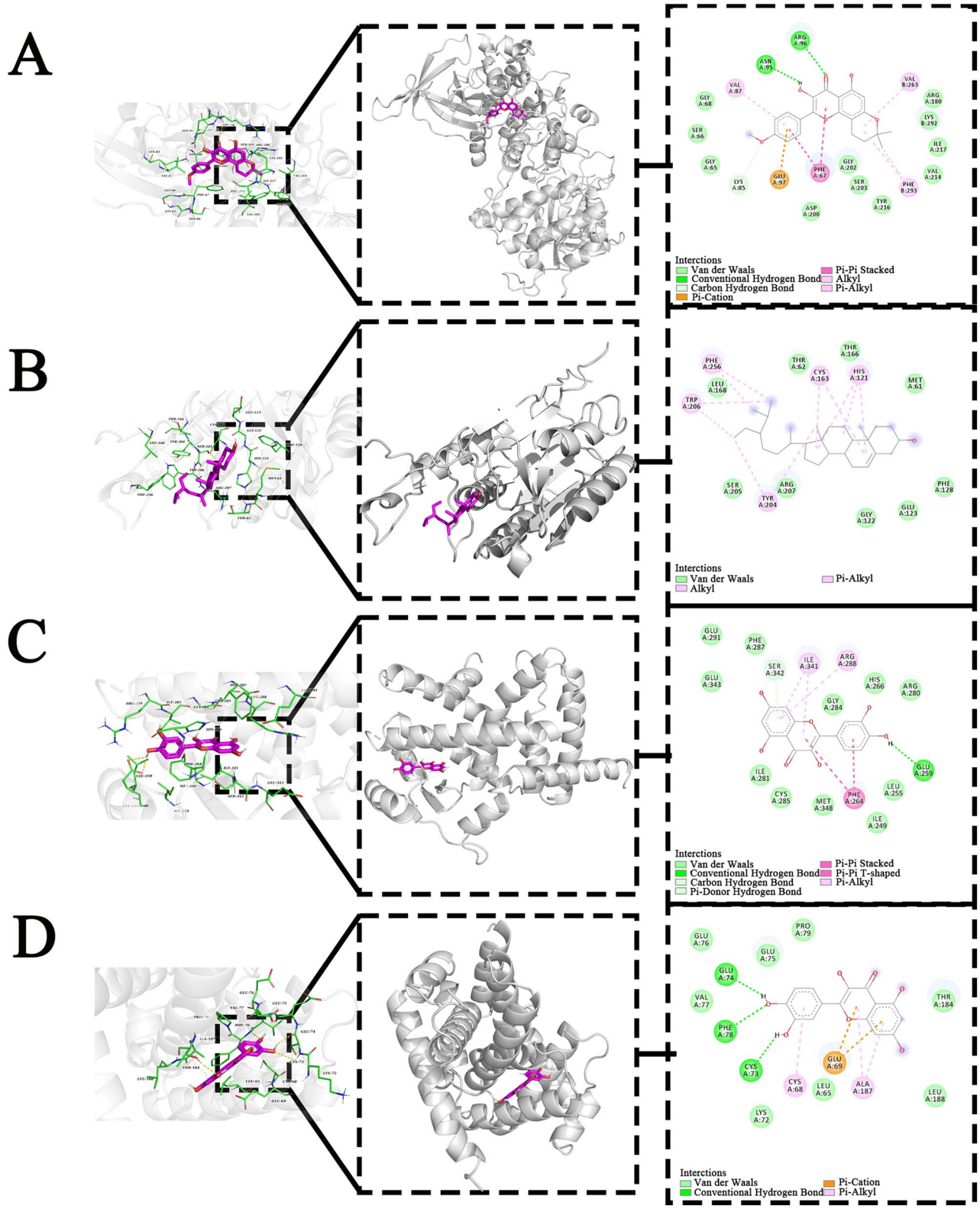

Fig. 7 Representation of the interaction between the *S. glabra* component with target proteins. left side, illustrate the interactions in a three-dimensional format, while on the right side, depict the same interaction in a two-dimensional format. **A**: GSK3B/anhydroicaritin. **B**: CASP3/beta-sitosterol. **C**: PPARG/quercetin. **D**: CCND1/quercetin

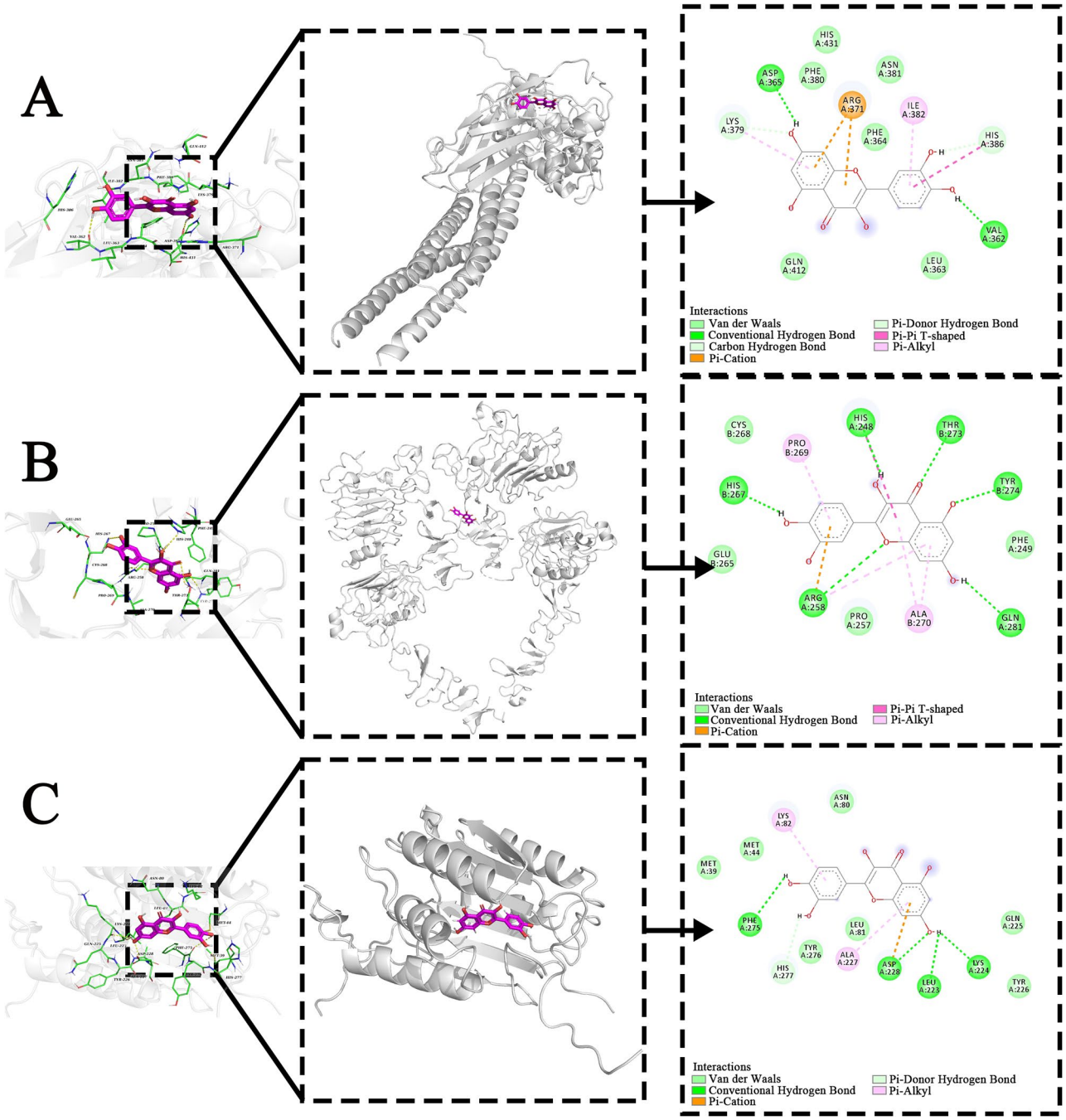

Fig. 8 Representation of the interaction between the quercetin with target proteins. left side, illustrate the interactions in a three-dimensional format, while on the right side, depict the same interaction in a two-dimensional format. **A**: STAT1/quercetin. **B**: ERBB2/quercetin. **C**: CASP3/quercetin

with the small molecules, the contribution of each residue to the total binding free energy was analyzed. The EMM values of residues with significant contributions. In the GSK3B-anhydroicaritin complex, Phe67 and Arg96 had the highest EMM values (Fig. 9B). In the PPARG-quercetin complex, His266 and Ile341 in the hinge region had the highest EMM values (Fig. 10B).

The RMSF values of backbone atoms in the GSK3B-anhydroicaritin and PPARG-quercetin complexes were calculated to analyze the fluctuation and stability of key residues in the active pocket site. The RMSF values of both complexes were < 0.5 nm, with the GSK3B-anhydroicaritin complex showing smaller values. Overall, RMSD values remained within a narrow range, indicating strong binding stability between the protein and small molecules (Figs. 9C and 10C).

In MD simulations, the radius of gyration (Rg) is a key parameter that reflects the compactness and spatial

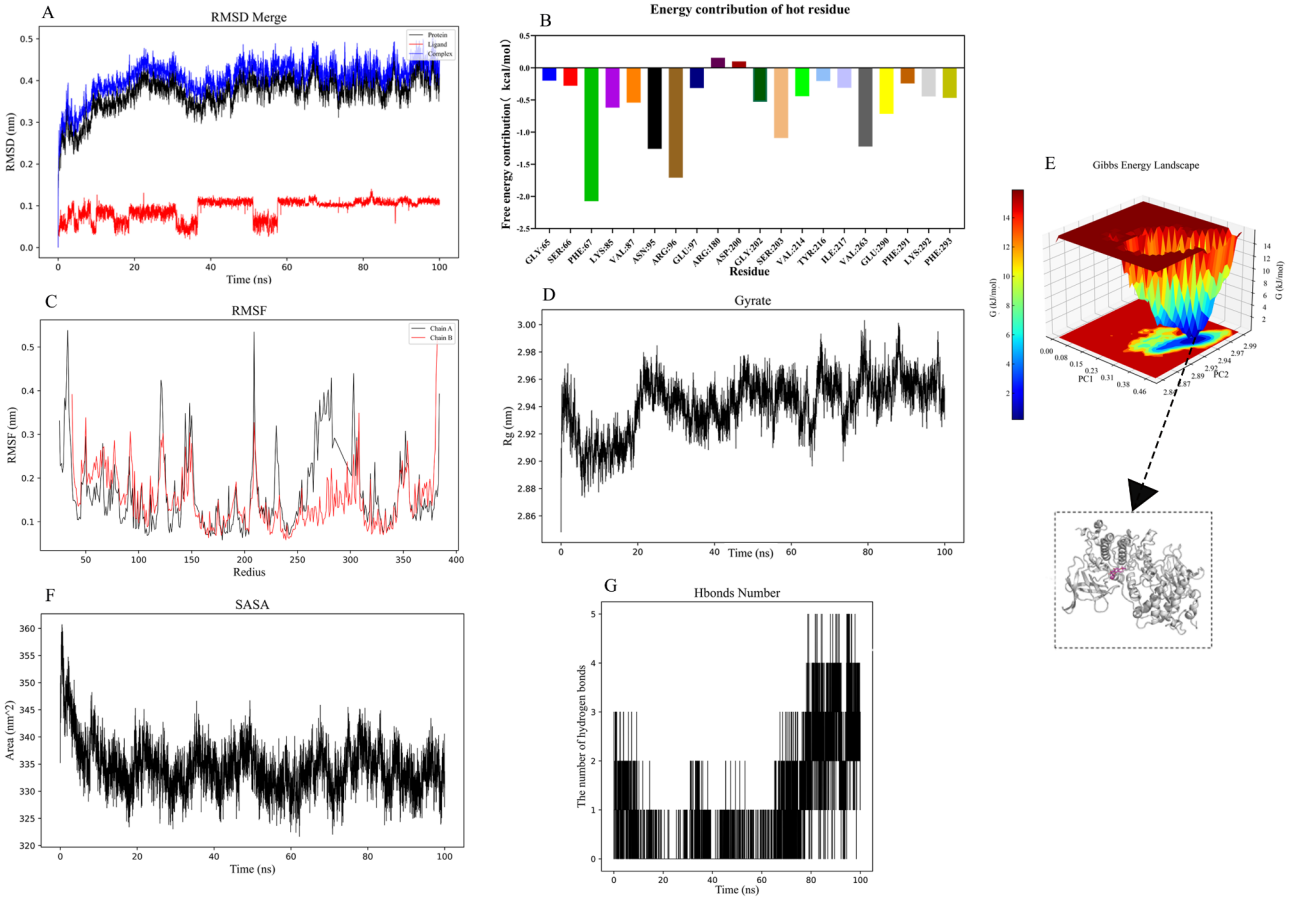

Fig. 9 Molecular dynamics simulation analysis results of GSK3B/anhydroicaritin. **A**: RMSD of small molecules and proteins in the simulated 100 ns process. **B**: Energy contribution of hot residue of small molecules and proteins in the simulated 100 ns process. **C**: Simulated root mean square fluctuations (RMSF) of small molecules and proteins. **D**: Simulated radii of gyration (Rg) of protein backbone atoms during 100 ns. **E**: Gibbs energy landscape of GSK3B/anhydroicaritin. **F**: solvent-accessible surface area (SASA) of GSK3B/anhydroicaritin. **G**: Hbonds number of GSK3B/anhydroicaritin

occupancy of a complex system. The Rg curves of protein–small molecule complexes analyzed in this study. The Rg curve of the GSK3B-anhydroicaritin complex stabilized between 20 and 100 ns, fluctuating within the range of 2.92–2.98 without significant deviation (Fig. 9D). Similarly, the Rg curve of the PPARG-quercetin complex reached an equilibrium between 40 and 100 ns, fluctuating within the range of 1.93–1.96 with minimal variance (Fig. 10D). These results indicated that the small molecules and proteins had high binding affinity.

Free energy landscapes (FELs) are graphical representations of biomolecular interactions, in which energy traps manifest as valleys upon molecular binding. Both GSK3B-anhydroicaritin and PPARG-quercetin complexes exhibited a single energy trap. At the lowest energy trap, the conformations of both complexes were in a tightly bound state (Figs. 9E and 10E). In addition, the FEL demonstrated that both complexes had more stable binding, suggesting that anhydroicaritin and quercetin from *S. glabra* are promising drugs for the treatment of PC.

MD simulations have shown a correlation between the solvent-accessible surface area (SASA) and protein stability. The SASA of the GSK3B-anhydroicaritin complex stabilized at approximately 20 ns, with an equilibrium value of approximately 333 nm^2 (Fig. 9F). Similarly, the SASA of the PPARG-quercetin complex stabilized at approximately 40 ns, with an equilibrium value of approximately 144 nm2 (Fig. 10F). These findings suggested that the interactions between the small molecules and proteins contributed to the stability of the protein structure.

Hydrogen bonding significantly influences the stability of a protein structure. The HBond diagrams (Figs. 9G and 10G) of the GSK3B-anhydroicaritin and PPARG-quercetin complexes indicated the formation of numerous hydrogen bonds between the proteins and small molecules, primarily involving key residues in the proteins and important groups in the small molecules. These findings highlight the crucial role of hydrogen bonding in facilitating the interaction between small molecules and proteins.

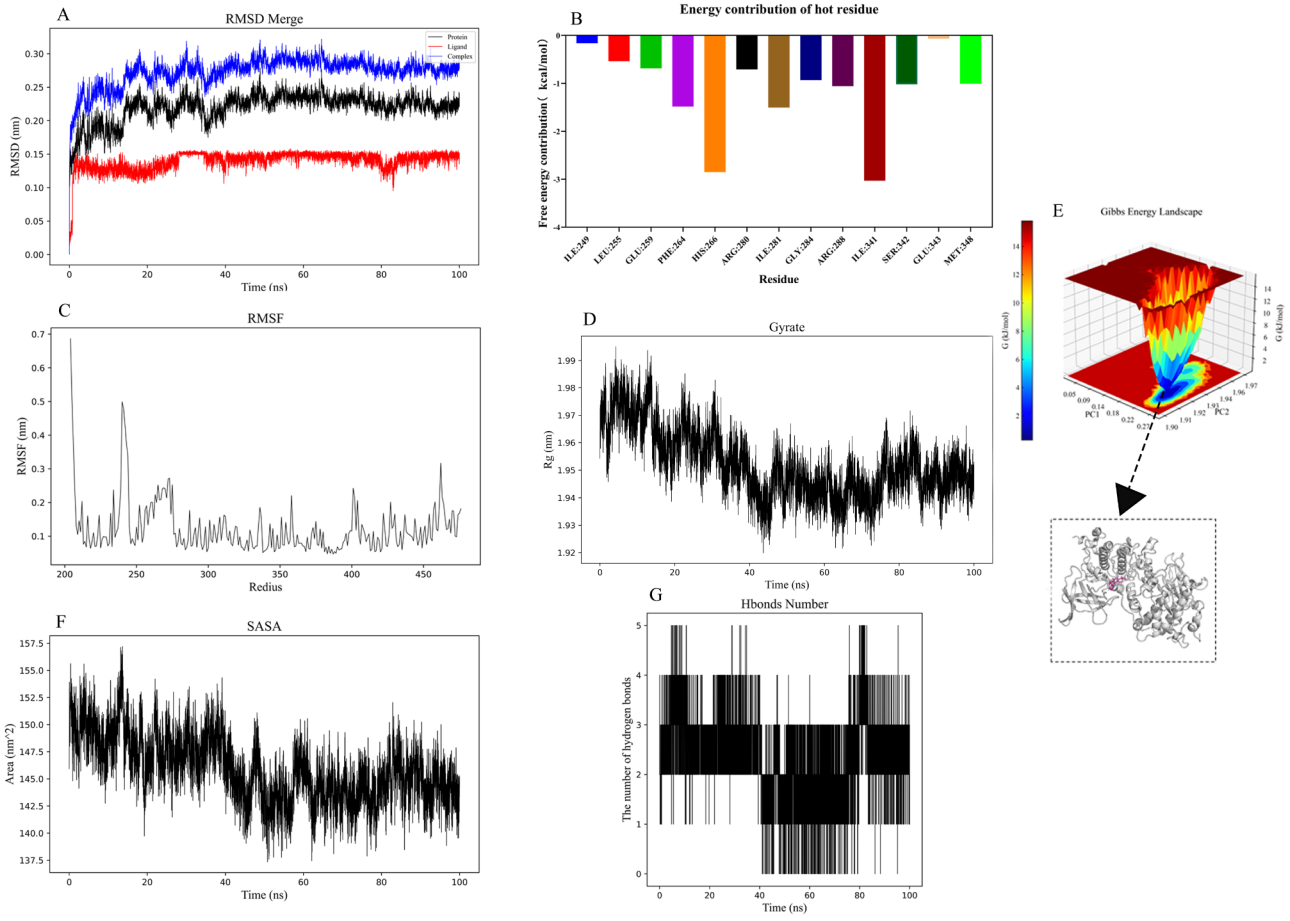

Fig. 10 Molecular dynamics simulation analysis results of PPARG/quercetin. **A**: RMSD of small molecules and proteins in the simulated 100 ns process. **B**: Energy contribution of hot residue of small molecules and proteins in the simulated 100 ns process. **C**: Simulated root mean square fluctuations (RMSF) of small molecules and proteins. **D**: Simulated radii of gyration (Rg) of protein backbone atoms during 100 ns. **E**: Gibbs energy landscape of PPARG/quercetin. **F**: solvent-accessible surface area (SASA) of PPARG/quercetin. **G**: Hbonds number of PPARG/quercetin

Table 3 Protein ligand MMPBSA analysis(KCal/Mol)

	GSK3B-Anhydroicaritin	PPARG-Quercetin
VDWAALS	-45.70 ± 0.92	-35.39 ± 0.61
EEL	-19.65 ± 0.77	-38.97 ± 4.34
EGB	38.32 ± 0.51	45.05 ± 1.39
ESURF	-6.08 ± 0.00	-5.01 ± 0.04
ΔGgas	-65.36 ± 1.20	-74.36 ± 4.38
ΔGsolv	32.24 ± 0.51	40.04 ± 1.39
ΔTOTAL	-33.12 ± 1.31	-34.32 ± 4.60

The stability of protein–ligand binding was validated by analyzing the displacement of simulated trajectories of anhydroicaritin and quercetin at various time points. If protein–ligand binding is stable, the positions of the ligand and receptor should remain relatively unchanged over time. In this study, we initially compared the conformations of anhydroicaritin with GSK3B or quercetin with PPARG at 0 ns, and subsequently evaluated the changes in relative position at different time points. No significant changes in the conformational positions of GSK3B-anhydroicaritin and PPARG-quercetin were observed during the first 100 ns of the kinetic simulation, suggesting that the GSK3B-anhydroicaritin and PPARG-quercetin complexes had stable binding (Supplement movie 1 and 2, Additional File 6). The binding of small molecules leads to a more compact structure of the protein, reduced surface area, and formation of multiple hydrogen bonds with the protein.

Validation of the anti-pancreatic cancer effects of *S. glabra* in vitro

In vitro experiments were performed to validate the inhibitory effects of *S. glabra* on the proliferation of PC cells. The viability of PANC-1 cells was assessed after 48 h of exposure to increasing concentrations of *S. glabra* extracts. As shown Fig . 11A, S. *glabra* extracts significantly inhibited the growth of PANC-1 cells in a dose-dependent manner, with an IC50 value of 42.49 μg/mL, which indicated a notable anti-tumor effect. Furthermore, qRT-PCR was performed to evaluate the

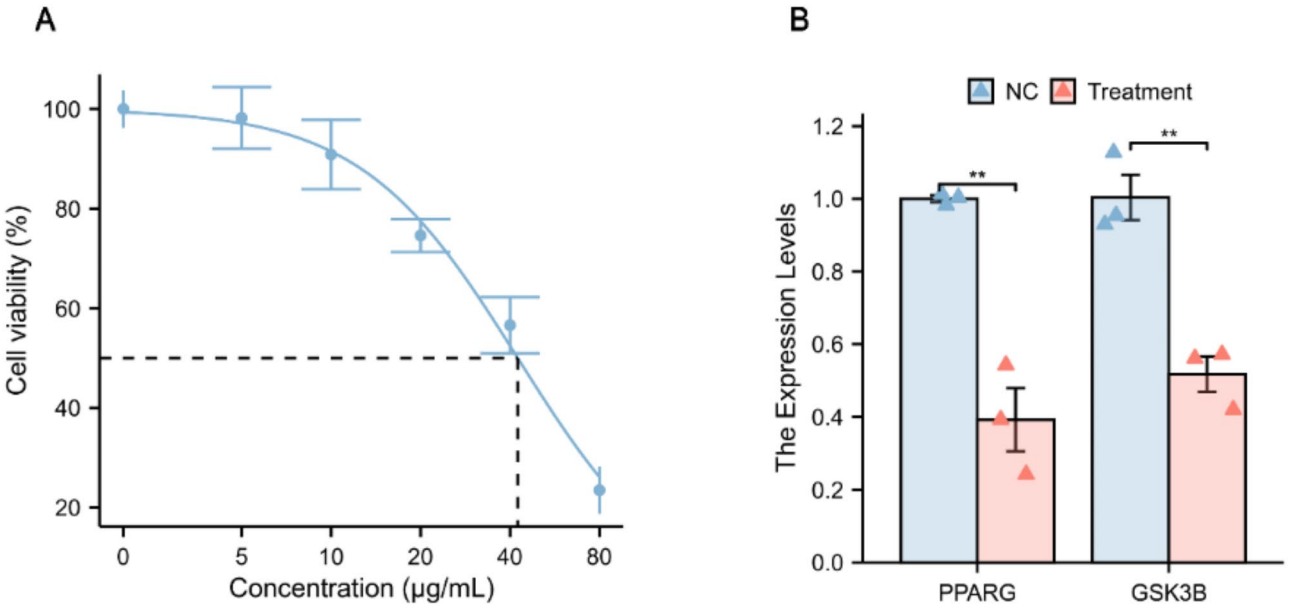

Fig. 11 Experimental verification of *S. glabra* against pancreatic cancer in vitro. **A**: Cell viability was measured after being treated with different concentration of *S. glabra* extracts for 48 h ($n=3$). **B**: qRT-PCR measured the mRNA levels of GSK3B and PPARG in PANC-1 cells treated with S. glabra extracts 30 μg/mL for 24 h ($n=3$)

expression of two hub target genes in PANC-1 cells treated with *S. glabra* extract at a concentration of 30 μg/mL for 24 h. As shown Fig . 11B, S. *glabra* extract effectively decreased the expression of *PPARG* and *GSK3B*, suggesting that it prevents the growth of PC cells by downregulating these genes synergistically.

Discussion

With the increasing recognition of TCM for its ability to control disease progression, alleviate clinical symptoms, and improve the quality of life of patients, the use of plant-derived components in anti-cancer treatment has gradually increased. *S. glabra* contains various active components with specific antitumor effects. An anti-tumor component found in *S. glabra* is rosmarinic acid, which has been shown to inhibit tumor cell proliferation and migration, induce apoptosis, downregulate Bcl-2, and upregulate Bax in breast cancer [36]. However, the therapeutic value of *S. glabra* in PC remains unclear, emphasizing the requirement for a more comprehensive investigation into the multi-target therapeutic mechanisms of *S. glabra*.

TCM has demonstrated satisfactory clinical efficacy in treating complex diseases through a "multi-component, multi-target, and multi-pathway" approach. Network pharmacology has emerged as a promising approach to advancing drug discovery and elucidating the mechanisms of action of multi-target compounds [37]. Modern technologies such as microarray, sequencing, and other bioinformatic tools have facilitated the identification of oncogenes, underlying mechanisms, tumor biomarkers, prognostic factors, and therapeutic targets [38, 39]. Network pharmacology and bioinformatics can be integrated to investigate drug–target interactions and the mechanisms of action of *S. glabra* to identify the most effective active component for treating PC.

This study revealed the active components of *S. glabra* and their target genes for the treatment of PC. Targeting genes involved in cancer-related pathways may facilitate disease management. *BAX*, *CCND1*, *BCL2L1*, *EGF*, *STAT1*, *ERBB2*, and *RAC1* were directly associated with PC, indicating that dysregulation of these genes may lead to the development of PC. The results section mentions composite target network showed that beta-sitosterol, sitosterol, anhydroicaritin, engelitin, propionic acid, istanbulin A, ZINC00391893, chloranthalactone A, quercetin, atractylenolide II, atractylenolide III, fumaric acid, mipax, phytodolor, scoparone, scopoletol, vanillic acid, and caffeic acid exhibited strong interactions, indicating their potential anticancer properties. The target genes *CASP3*, *MMP9*, *CCND1*, *EGF*, *MMP2*, *CASP8*, *GSK3B*, *ERBB2*, *STAT1*, and *PPARG* were identified as DEGs in three microarray datasets from the GEO database (GSE15471, GSE28732, and GSE62452). In addition, KM analysis showed that the gene expression of *CASP3*, *CCND1*, *GSK3B*, *ERBB2*, *STAT1*, and *PPARG* were associated with the survival of patients with PC.

Glycogen synthase kinase 3 beta (GSK3β) is a highly conserved serine/threonine kinase that plays a crucial role in regulating various cellular processes, such as cell proliferation, DNA repair, cell cycle progression, signaling, and metabolism. Recent studies have shown that

GSK3β is a potential therapeutic target for PDAC owing to its involvement in promoting tumor transformation, tumor cell survival, and resistance to chemotherapy [40]. Notably, higher GSK3β expression is associated with shorter survival in patients with PDAC, validating that GSK3β is involved in the progression of PDAC [41, 42]. In this study, *S. glabra* extract was found to inhibit the expression of GSK3B in PC cells in vitro, providing a foundation for further investigation into the pharmacological mechanism of *S. glabra* in PC.

Peroxisome proliferator-activated receptor-gamma (PPARG) is a nuclear receptor that functions as a transcription factor involved in regulating energy metabolism, cell cycle, cell differentiation, and apoptosis. Owing to these unique properties, PPARG possesses significant therapeutic value [43]. Inactivation of PPARG has been shown to enhance the effectiveness of αPD-L1 and αPD-1 antibodies in treating mammary tumors in mice [44]. Upregulated PPARG is associated with a poor prognosis and promotes metastasis in various cancers, including human renal cell carcinoma, prostate cancer (nude mouse xenografts), and brain cancer (cell cultures) [45]. Regulating the activity of PPARG may represent a therapeutic strategy for PC. Consistently, this study showed that higher PPARG expression was associated with a worse prognosis in PC. Cellular experiments showed that *S. glabra* extracts effectively inhibited PPARG expression, offering a potential avenue for prolonging patient survival.

Molecular docking is a common computer-based method used in drug discovery, particularly in identifying the potential targets of active components of Chinese herbs [46]. Unlike traditional pharmacological experiments, which were limited by cost and other factors, computer-aided drug design allows for large-scale screening and validation [47, 48]. In this study, quercetin was found to bind to PPARG stably, therefore, quercetin is a promising PPARG inhibitor that can be used in the treatment of PC. Additionally, anhydroicaritin could stably bind to GSK3B, suggesting its potential as an effective drug for the treatment of PC. MD simulation is a robust computational tool used to analyze the dynamic interactions between targets and small molecules, providing valuable insights into the mechanisms of action of the molecules and guiding drug design. Despite its strengths, MD simulation has certain limitations as a virtual validation method, emphasizing the requirement of further validation of molecular docking results through in vitro experiments. In this study, in vitro experiments showed that *S. glabra* extracts effectively inhibited the proliferation of PC cells. In addition, qRT-PCR result showed that *S. glabra* extracts suppressed the expression of *PPARG* and *GSK3B*, two target genes of *S. glabra* identified via network pharmacological analysis, in PC cells. These results validated the accuracy of the results of network pharmacology, molecular docking, and MD simulations.

Altogether, this study provides a theoretical foundation for assessing the therapeutic value of the active components of *S. glabra* in PC. A combination of network pharmacology and bioinformatic analysis was used to elucidate the complex mechanism of action of *S. glabra* in the treatment of PC. Although the findings were validated using gene expression data, survival analysis, molecular docking, and in vitro experiments, this study has several limitations. First, further in vivo experiments are warranted to validate the results. Second, the use of larger datasets containing information on traditional drugs and target genes may enhance the accuracy of network pharmacological analysis. Third, despite integrating network pharmacology with molecular docking, the precise therapeutic mechanism of action of *S. glabra* in PC could not be comprehensively determined. Therefore, a multidisciplinary approach is required to gain a comprehensive understanding of the therapeutic potential of *S. glabra* in PC.

Conclusion

Pancreatic cancer, a prevalent malignant tumor of the digestive system, is difficult to treat owing to drug resistance and hence has a low survival rate. Unlike previous studies on TCM, this study employed a computer-aided drug design approach for high-throughput screening of the active components and target genes of *S. glabra* for the treatment of PC. Potential therapeutic components were identified using TCM databases and a literature search. Furthermore, network pharmacology and bioinformatic analysis were integrated to elucidate the mechanism of action of *S. glabra* in the treatment of PC. The findings were validated using microarray data, survival analysis, molecular docking, MD simulations, and in vitro experiments. β-sitosterol, quercetin, and anhydroicaritin were identified as potential therapeutic compounds, with their targets being associated with the survival of patients with PC. *STAT1*, *ERBB2*, *GSK3B*, *PPARG*, *CCND1*, and *CASP3* were identified as potential therapeutic targets for PC patients survival. In conclusion, this study highlights the multi-target and multi-pathway therapeutic effects of *S. glabra* against PC. The use of advanced virtual screening and MD simulation to assess the impact of plant-derived compounds on PC is a noteworthy advancement towards the modernization and globalization of TCM. In addition, this integrated method may improve drug design and discovery, decrease experimental expenses, and promote scientific and technological advancements in the field.

Supplementary Information

The online version contains supplementary material available at https://doi.org/10.1186/s12906-025-04839-5.

Supplementary Material 1

Supplementary Material 2

Supplementary Material 3

Supplementary Material 4

Supplementary Material 5

Supplementary Material 6

Acknowledgements
Not applicable.

Author contributions
Xing Liu wrote the main manuscript text and Jianghong Ou prepared all figures. All authors reviewed the manuscript.

Funding
This work was supported by the National Natural Science Foundation of China (Grants 82304796).

Data availability
The analyzed data sets generated during the study are available from the corresponding author on reasonable request.

Declarations

Ethics approval and consent to participate
Not applicable.

Consent for publication
Not applicable.

Competing interests
The authors declare no competing interests.

Author details
[1]Department of Pharmacy, Beijing Friendship Hospital, Capital Medical University, Beijing 100050, China
[2]Department of Integrated Chinese and Western Medicine, The Affiliated Changsha Central Hospital, Hengyang Medical School, University of South China, Changsha 410004, China

Received: 5 November 2024 / Accepted: 26 February 2025
Published online: 17 March 2025

References

1. Siegel RL, Giaquinto AN, Jemal A. Cancer statistics. Cancer J Clin. 2024;74(2024):12–49. https://doi.org/10.3322/caac.21820
2. Xia C, Dong X, Li H, Cao M, Sun D, He S, Yang F, Yan X, Zhang S, Li N, Chen W. Cancer statistics in China and united States, 2022: profiles, trends, and determinants. Chin Med J. 2022;135:584–90. https://doi.org/10.1097/cm9.0000000000002108
3. Rahib L, Smith BD, Aizenberg R, Rosenzweig AB, Fleshman JM, Matrisian LM. Projecting cancer incidence and deaths to 2030: the unexpected burden of thyroid, liver, and pancreas cancers in the united States. Cancer Res. 2014;74:2913–21. https://doi.org/10.1158/0008-5472.Can-14-0155
4. The global. regional, and national burden of pancreatic cancer and its attributable risk factors in 195 countries and territories, 1990–2017: a. Gastroenterol Hepatol. 2019;4:934–47. https://doi.org/10.1016/s2468-1253(19)30347-4. systematic analysis for the Global Burden of Disease Study 2017, The lancet.
5. Kleeff J, Reiser C, Hinz U, Bachmann J, Debus J, Jaeger D, Friess H, Büchler MW. Surgery for recurrent pancreatic ductal adenocarcinoma. Ann Surg. 2007;245:566–72. https://doi.org/10.1097/01.sla.0000245845.06772.7d
6. Chu JN, Krishnan P, Lim KH. A comprehensive review on the chemical constituents, sesquiterpenoid biosynthesis and biological activities of Sarcandra glabra. Nat Prod Bioprospecting. 2023;13:53. https://doi.org/10.1007/s13659-023-00418-8
7. Zeng Y, Liu J, Zhang Q, Qin X, Li Z, Sun G, Jin S. The traditional uses, phytochemistry and Pharmacology of Sarcandra glabra (Thunb.) Nakai, a Chinese herb with potential for development. Rev Front Pharmacol. 2021;12:652926. https://doi.org/10.3389/fphar.2021.652926
8. Hopkins AL. Network Pharmacology. Nat Biotechnol. 2007;25:1110–1. https://doi.org/10.1038/nbt1007-1110
9. Hopkins AL. Network pharmacology: the next paradigm in drug discovery. Nat Chem Biol. 2008;4:682–90. https://doi.org/10.1038/nchembio.118
10. Li S, Zhang B. Traditional Chinese medicine network pharmacology: theory, methodology and application. Chin J Nat Med. 2013;11:110–20. https://doi.org/10.1016/s1875-5364(13)60037-0
11. Nogales C, Mamdouh ZM, List M, Kiel C, Casas AI, Schmidt H. Network pharmacology: curing causal mechanisms instead of treating symptoms. Trends Pharmacol Sci. 2022;43:136–50. https://doi.org/10.1016/j.tips.2021.11.004
12. Wang S, Gao J, Li Q, Ming W, Fu Y, Song L, Qin J. Study on the regulatory mechanism and experimental verification of Icariin for the treatment of ovarian cancer based on network Pharmacology. J Ethnopharmacol. 2020;262:113189. https://doi.org/10.1016/j.jep.2020.113189
13. Zhang Q, Liu J, Li R, Zhao R, Zhang M, Wei S, Ran D, Jin W, Wu C. A network Pharmacology approach to investigate the anticancer mechanism and potential active ingredients of Rheum palmatum L. Against lung Cancer via induction of apoptosis. Front Pharmacol. 2020;11:528308. https://doi.org/10.3389/fphar.2020.528308
14. Ru J, Li P, Wang J, Zhou W, Li B, Huang C, Li P, Guo Z, Tao W, Yang Y, Xu X, Li Y, Wang Y, Yang L. TCMSP: a database of systems Pharmacology for drug discovery from herbal medicines. J Cheminform. 2014;6:13. https://doi.org/10.1186/1758-2946-6-13
15. Shi WB, Wang ZX, Liu HB, Jia YJ, Wang YP, Xu X, Zhang Y, Qi XD, Hu FD. Study on the mechanism of Fufang E'jiao Jiang on precancerous lesions of gastric cancer based on network Pharmacology and metabolomics. J Ethnopharmacol. 2023;304:116030. https://doi.org/10.1016/j.jep.2022.116030
16. Yang PW, Xu PL, Cheng CS, Jiao JY, Wu Y, Dong S, Xie J, Zhu XY. Integrating network Pharmacology and experimental models to investigate the efficacy of QYHJ on pancreatic cancer. J Ethnopharmacol. 2022;297:115516. https://doi.org/10.1016/j.jep.2022.115516
17. Chen FY, Chen ZC, Luo YM. [Research progress on chemical constituents and biological activities of Sarcandra glabra], Zhongguo Zhong Yao Za zhi = zhongguo Zhongyao Zazhi = China. J Chin Materia Med. 2022;47:872–9. https://doi.org/10.19540/j.cnki.cjcmm.20211012.201
18. Badea L, Herlea V, Dima SO, Dumitrascu T, Popescu I. Combined gene expression analysis of whole-tissue and microdissected pancreatic ductal adenocarcinoma identifies genes specifically overexpressed in tumor epithelia. Hepatogastroenterology. 2008;55:2016–27.
19. Zhang G, Schetter A, He P, Funamizu N, Gaedcke J, Ghadimi BM, Ried T, Hassan R, Yfantis HG, Lee DH, Lacy C, Maitra A, Hanna N, Alexander HR, Hussain SP. DPEP1 inhibits tumor cell invasiveness, enhances chemosensitivity and predicts clinical outcome in pancreatic ductal adenocarcinoma. PLoS ONE. 2012;7:e31507. https://doi.org/10.1371/journal.pone.0031507
20. Yang S, He P, Wang J, Schetter A, Tang W, Funamizu N, Yanaga K, Uwagawa T, Satoskar AR, Gaedcke J, Bernhardt M, Ghadimi BM, Gaida MM, Bergmann F, Werner J, Ried T, Hanna N, Alexander HR, Hussain SP. A novel MIF signaling pathway drives the malignant character of pancreatic Cancer by targeting NR3C2, Cancer research, 2016;76:3838–50. https://doi.org/10.1158/0008-5472.Can-15-2841
21. Chen H, Boutros PC. VennDiagram: a package for the generation of highly-customizable Venn and Euler diagrams in R. BMC Bioinformatics. 2011;12:35. https://doi.org/10.1186/1471-2105-12-35
22. UniProt: the Universal Protein Knowledgebase in 2023, Nucleic acids research, 2023;51:D523-d531. https://doi.org/10.1093/nar/gkac1052
23. Szklarczyk D, Kirsch R, Koutrouli M, Nastou K, Mehryary F, Hachilif R, Gable A.L., Fang T, Doncheva N.T., Pyysalo S., Bork P., Jensen L.J., von Mering C. The STRING database in 2023: protein-protein association networks and functional enrichment analyses for any sequenced genome of interest. Nucleic Acids Res. 2023;51:D638–46. https://doi.org/10.1093/nar/gkac1000

24. Shannon P, Markiel A, Ozier O, Baliga NS, Wang JT, Ramage D, Amin N, Schwikowski B, Ideker T. Cytoscape: a software environment for integrated models of biomolecular interaction networks. Genome Res. 2003;13:2498–504. https://doi.org/10.1101/gr.1239303
25. Chin CH, Chen SH, Wu HH, Ho CW, Ko MT, Lin CY. CytoHubba: identifying hub objects and sub-networks from complex interactome. BMC Syst Biol. 2014;8 Suppl 4:S11. https://doi.org/10.1186/1752-0509-8-s4-s11
26. Huang da W, Sherman BT, Lempicki RA. Systematic and integrative analysis of large gene lists using DAVID bioinformatics resources. Nat Protoc. 2009;4:44–57. https://doi.org/10.1038/nprot.2008.211
27. Liu J, Lichtenberg T, Hoadley KA, Poisson LM, Lazar AJ, Cherniack AD, Kovatich AJ, Benz CC, Levine DA, Lee AV, Omberg L, Wolf DM, Shriver CD, Thorsson V, Hu H. An integrated TCGA Pan-Cancer clinical data resource to drive High-Quality survival outcome analytics, cell, 2018;173:400–e416411. https://doi.org/10.1016/j.cell.2018.02.052
28. Mayakonda A, Lin DC, Assenov Y, Plass C, Koeffler HP. Maftools: efficient and comprehensive analysis of somatic variants in cancer. Genome Res. 2018;28:1747–56. https://doi.org/10.1101/gr.239244.118
29. Bindea G, Mlecnik B, Tosolini M, Kirilovsky A, Waldner M, Obenauf AC, Angell H, Fredriksen T, Lafontaine L, Berger A, Bruneval P, Fridman WH, Becker C, Pagès F, Speicher MR, Trajanoski Z, Galon J. Spatiotemporal dynamics of intratumoral immune cells reveal the immune landscape in human cancer, immunity, 2013;39:782–95. https://doi.org/10.1016/j.immuni.2013.10.003
30. Burley SK, Bhikadiya C, Bi C, Bittrich S, Chao H, Chen L, Craig PA, Crichlow GV, Dalenberg K, Duarte JM, Dutta S, Fayazi M, Feng Z, Flatt JW, Ganesan SJ, Ghosh S, Goodsell DS, Green RK, Guranovic V, Henry J, Hudson BP, Khokhriakov I, Lawson CL, Liang Y, Lowe R, Peisach E, Persikova I, Piehl DW, Rose Y, Sali A, Segura J, Sekharan M, Shao C, Vallat B, Voigt M, Webb B, Westbrook JD, Whetstone S, Young JY, Zalevsky A, Zardecki C. RCSB protein data bank: tools for visualizing and Understanding biological macromolecules in 3D, protein science: a publication of the protein society, 2022;31:e4482. https://doi.org/10.1002/pro.4482
31. Krause F, Voigt K, Di Ventura B, Öztürk MA. ReverseDock: a web server for blind Docking of a single ligand to multiple protein targets using AutoDock Vina. Front Mol Biosci. 2023;10:1243970. https://doi.org/10.3389/fmolb.2023.1243970
32. Mooers BHM. Shortcuts for faster image creation in PyMOL. Protein Science: Publication Protein Soc. 2020;29:268–76. https://doi.org/10.1002/pro.3781
33. Gruber CC, Pleiss J. Systematic benchmarking of large molecular dynamics simulations employing GROMACS on massive multiprocessing facilities. J Comput Chem. 2011;32:600–6. https://doi.org/10.1002/jcc.21645
34. Van Der Spoel D, Lindahl E, Hess B, Groenhof G, Mark AE, Berendsen HJ. GROMACS: fast, flexible, and free. J Comput Chem. 2005;26:1701–18. https://doi.org/10.1002/jcc.20291
35. Adasme MF, Linnemann KL, Bolz SN, Kaiser F, Salentin S, Haupt VJ, Schroeder M. PLIP 2021: expanding the scope of the protein-ligand interaction profiler to DNA and RNA. Nucleic Acids Res. 2021;49:W530–4. https://doi.org/10.1093/nar/gkab294
36. Li H, Zhuang HL, Lin JJ, Zhang YF, Huang H, Luo T, Yu WT, Ni F. Effect of Rosmarinic acid from Sarcandra glabra in inhibiting proliferation and migration and inducing apoptosis of MDA-MB-231 cells via regulation of expressions of Bcl-2 and Bax. Zhongguo Zhong Yao Za Zhi = Zhongguo Zhongyao Zazhi = China J Chin Materia Med. 2018;43:3335–40. https://doi.org/10.19540/j.cnki.cjcmm.20180508.001
37. Li L, Yang L, Yang L, He C, He Y, Chen L, Dong Q, Zhang H, Chen S, Li P. Network pharmacology: a bright guiding light on the way to explore the personalized precise medication of traditional Chinese medicine. Chin Med. 2023;18:146. https://doi.org/10.1186/s13020-023-00853-2
38. Li C, Yang L, Zhang Y, Hou Q, Wang S, Lu S, Tao Y, Hu W, Zhao L. Integrating single-cell and bulk transcriptomic analyses to develop a cancer-associated fibroblast-derived biomarker for predicting prognosis and therapeutic response in breast cancer. Front Immunol. 2023;14:1307588. https://doi.org/10.3389/fimmu.2023.1307588
39. Dantas E, Murthy A, Ahmed T, Ahmed M, Ramsamooj S, Hurd MA, Lam T, Malbari M, Agrusa C, Elemento O, Zhang C, Pappin DJ, McGraw TE, Stiles BM, Altorki NK, Goncalves MD. TIMP1 is an early biomarker for detection and prognosis of lung cancer, clinical and translational medicine, 2023;13:e1391. https://doi.org/10.1002/ctm2.1391
40. Ding L, Madamsetty VS, Kiers S, Alekhina O, Ugolkov A, Dube J, Zhang Y, Zhang JS, Wang E, Dutta SK, Schmitt DM, Giles FJ, Kozikowski AP, Mazar AP, Mukhopadhyay D, Billadeau DD. Glycogen synthase Kinase-3 Inhibition sensitizes pancreatic Cancer cells to chemotherapy by abrogating the TopBP1/ATR-Mediated DNA damage response. Clin cancer Research: Official J Am Association Cancer Res. 2019;25:6452–62. https://doi.org/10.1158/1078-0432.Ccr-19-0799
41. Ougolkov AV, Fernandez-Zapico ME, Bilim VN, Smyrk TC, Chari ST, Billadeau DD. Aberrant nuclear accumulation of glycogen synthase kinase-3beta in human pancreatic cancer: association with kinase activity and tumor dedifferentiation. Clin cancer Research: Official J Am Association Cancer Res. 2006;12:5074–81. https://doi.org/10.1158/1078-0432.Ccr-06-0196
42. Nagini S, Sophia J, Mishra R. Glycogen synthase kinases: moonlighting proteins with theranostic potential in cancer. Sem Cancer Biol. 2019;56:25–36. https://doi.org/10.1016/j.semcancer.2017.12.010
43. Mrowka P, Glodkowska-Mrowka E. PPARγ agonists in combination Cancer therapies. Curr Cancer Drug Targets. 2020;20:197–215. https://doi.org/10.2174/1568009619666191209102015
44. Wu B, Sun X, Yuan B, Ge F, Gupta HB, Chiang HC, Li J, Hu Y, Curiel TJ, Li R. PPARγ Inhibition boosts efficacy of PD-L1 checkpoint Blockade immunotherapy against murine melanoma in a sexually dimorphic manner. Int J Biol Sci. 2020;16:1526–35. https://doi.org/10.7150/ijbs.42966
45. Zou Y, Watters A, Cheng N, Perry CE, Xu K, Alicea GM, Parris JLD, Baraban E, Ray P, Nayak A, Xu X, Herlyn M, Murphy ME, Weeraratna AT, Schug ZT, Chen Q. Polyunsaturated fatty acids from astrocytes activate PPARγ signaling in Cancer cells to promote brain metastasis, Cancer discovery, 2019;9:1720–35. https://doi.org/10.1158/2159-8290.Cd-19-0270
46. Pinzi L, Rastelli G. Molecular docking: shifting paradigms in drug discovery. Int J Mol Sci. 2019;20. https://doi.org/10.3390/ijms20184331
47. Sun Z, Wang Y, Pang X, Wang X, Zeng H. Mechanisms of Polydatin against spinal cord ischemia-reperfusion injury based on network pharmacology, molecular Docking and molecular dynamics simulation. Bioorg Chem. 2023;140:106840. https://doi.org/10.1016/j.bioorg.2023.106840
48. Arumugam GS, Sen A, Dash SS, Mitra K, Doble M, Rajaraman G, Gummadi SN. Arjunetin as a promising drug candidate against SARS-CoV-2: molecular dynamics simulation studies. J Biomol Struct Dyn. 2022;40:12358–79. https://doi.org/10.1080/07391102.2021.1970627

Publisher's note